Modeling of phosphate flux induced by flood resuspension on a macrotidal estuarine mudflat (Seine, France)

Jean-Marie Barrois, Valérie Mesnage, Édouard Metzger, Dominique Mouazé, Lionel Denis, Julien Deloffre

Marine Chemistry 265–266 (2024) 104427

Contents lists available at ScienceDirect

Marine Chemistry

journal homepage: www.elsevier.com/locate/marchem

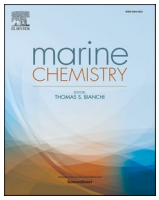

Modeling of phosphate flux induced by flood resuspension on a macrotidal estuarine mudflat (Seine, France)

Jean-Marie Barrois [a,*], Valérie Mesnage [a], Edouard Metzger [b], Dominique Mouazé [a], Lionel Denis [c], Julien Deloffre [a]

[a] Univ Rouen Normandie, Université Caen Normandie, CNRS, Normandie Univ, M2C UMR 6143, F-76000 Rouen, France
[b] UMR 6112 LPG, Université d'Angers, Nantes Université, Le Mans Université, CNRS, 49000 Angers, France
[c] UMR 8187 LOG, Université de Lille, Université du Littoral Côte d'Opale, Station Marine de Wimereux, CNRS, 59000 Lille, France.

ARTICLE INFO

Keywords:
Benthic flux
Modeling
Tidal resuspension
Phosphate
Seine estuary
Intertidal mudflat

ABSTRACT

Coastal marine sediments can be either major scrubbers or eutrophication contributors to surface waters. Standard methods for direct measurement of nutrient fluxes at the sediment-water interface do not consider hydrodynamic forcing although several *ex-situ* studies suggest that sediment resuspension can dramatically increase dissolved fluxes. We provide a new model to quantify dissolved phosphate (PO_4^{3-}) resuspension flux (J_R) based on physical representation of its identified components: diffusion stimulation by exposure of deeper sediment layer with higher PO_4^{3-} concentration in the porewater (J_D), pore water mixing with overlying water (J_M) and net adsorption/desorption from suspended sediments (J_K). This approach was applied to field data from a Seine intertidal mudflat periodically submitted to millimetric erosion. On a tidal scale, the model output reveals a J_R of 272.3 ± 360.0 μmol m^{-2} h^{-1} (± 52% from parameter uncertainty), well above flux calculated by application of Fick's first law (0.15 ± 0.85 μmol m^{-2} h^{-1}) or by *ex situ* core incubation (40.8 μmol m^{-2} h^{-1}). Iron bound phosphorus within suboxic layers buffers PO_4^{3-} concentrations in superficial sediments leading to negligible contributions of J_D and J_M to total fluxes. Conversely, J_K appears to be the main exchange pathway, even though improvements in turbidity measurement would allow this term to be defined more precisely. Correction required to enhance and control model robustness are described. These results show the importance of considering the dissolved PO_4^{3-} resuspension flux in dynamic environments.

1. Introduction

For shallow water bodies, limiting nutrients recycled from sediments constitute a source as large or much larger than external inputs (Boynton et al., 2008). In temperate latitudes, sediments can supply in excess the autotrophic phosphorus (P) demand (Boynton et al., 2018) leading to hypoxia (Mesnage et al., 2007) and harmful algal bloom (Yang et al., 2023). To quantify phosphate (PO_4^{3-}) flux at the sediment-water interface (SWI), the application of Fick's first law of diffusion or sediment incubation have been extensively used. However, these standard methods provide a steady-state measurement by isolating the sediment from its environment (Boynton et al., 2018), while hydrodynamic forcing - advection and sediment resuspension - becomes a major issue for results representativity in dynamic systems like estuaries (Denis et al., 2009). For example, advective flux has long been neglected in estuarine muddy sediments for practical reasons, although it is accepted that it is significant in permeable sandy sediments (Huettel et al., 2014). But more recently, Vennin (2018) has shown that pressure variation in a macrotidal estuary is sufficient to generate considerable advective flux despite low sediment permeability.

There are notably critical gaps concerning direct measurement of the dissolved PO_4^{3-} flux generated by sediment resuspension in macrotidal estuaries. Several *ex-situ* approaches have been used to simulate the impact of dredging, wind events or current resuspension on nutrients, oxygen and metals dynamics, including suspended extractions (Komada and Reimers, 2001; Schroeder et al., 2020), stirring microcosms (Reddy et al., 1996; Laima et al., 1998; You et al., 2007; Dunn et al., 2017), tank mesocosm (Porter et al., 2010) or wave flume (Sun et al., 2006; Zhu and Wang, 2014; Yu et al., 2017). Conclusions are divergent, PO_4^{3-} flux remains unchanged (Reddy et al., 1996), increases moderately compared to a conservative molecule Zhu and Wang, 2014) or increases dramatically after resuspension (Sun et al., 2006; Yu et al., 2017), because the

* Corresponding author.
E-mail address: barrois.jeanmarie@gmail.com (J.-M. Barrois).

https://doi.org/10.1016/j.marchem.2024.104427
Received 26 October 2023; Received in revised form 11 June 2024; Accepted 18 June 2024
Available online 19 June 2024

hydrodynamic constraints applied differ completely between studies. Therefore, they are not relevant for dynamic environments with variable forcing conditions. On the other hand, some *in situ* measurements have also been performed, with modified benthic chamber generating artificial resuspension (Tengberg et al., 2003) or by direct observation possible in closed waters (*e.g.,* Lake Tahiu, Zhu et al., 2005). However, there is still a lack of *in situ* flux measurements after natural resuspension in open waters. Although these previous experiments cannot fully reproduce *in situ* conditions, they enable identification of the transfer processes involved: (i) diffusive flux can be temporarily stimulated after erosion of superficial sediments (Porter et al., 2006; Hulot et al., 2023); (ii) Sun et al. (2006) have estimated that 8.5% of the dissolved PO_4^{3-} resuspension flux results from the interstitial waters mixing; and (iii) fast sorption kinetics - minute to hour - between suspended sediments and water column (Froelich, 1988) appears to control aqueous PO_4^{3-} concentration at resuspension time scale (Zhu and Wang, 2014; Yu et al., 2017). These observations can be used for model development, offering the possibility of an integrated approach to establish quantitative budgets in such a dynamic environment.

The macrotidal Seine estuary is one of the main estuaries of the North-West European continental shelf, and concentrates major socio-economic interests (Lafite and Romana, 2001). Phosphorus became the limiting element for primary production after the improvement of sewage treatment in the 2000s (Morelle, 2020). However, there are only few standard measurements of PO_4^{3-} flux at SWI (Bally et al., 2004). Progress has been made regarding advective flux (Vennin, 2018) but there is still no data on sediment resuspension flux while mudflats are frequently submitted to millimetric erosions (Deloffre et al., 2006). In this work, we provide a model for dissolved PO_4^{3-} resuspension flux measurements applied to high-resolution data from Seine intertidal mudflat, coupling acoustic submersible recording altimeter (Altus; Deloffre et al., 2005), PO_4^{3-} distribution on dissolved equilibrium in thin film (DET; Davison et al., 1991) and sorption batch experiment. Model outputs were used to assess: (1) the magnitude of the resuspension pathway compared to standard methods measurements; (2) the relative importance of transfer processes involved; and (3) the improvements required to mitigate model biases.

2. Material and methods

2.1. Study site and sampling

The "Tancarville mudflat" is an intertidal mudflat located in the mesohaline zone of the macrotidal Seine estuary (Fig. 1; N 49°28′16″ E 0°28′2″). This part of the estuary is under the influence of both tides and river flow, and the locus of turbidity maximum. The survey period from March to May 2022 includes 80 semi-diurnal tides up to 5 m tidal range and occurred during low-water period (378 m^{-3} s^{-1} on average; hydro.eaufrance.fr/stationhydro/H320000104). Sampling was carried out at neap tide on 11.04.2022 (tidal coefficient = 31; maree.shom.fr/harbor/HONFLEUR). Core sediments were retrieved by hand at low tide on station A (3 and 8 cm inner diameter for geochemical and physico-chemical characterization, 26 cm inner diameter for incubation and DET measurements). Surface waters were collected during flood tide on station W, 20 m from shore (Fig. 1). Temperature (14.2 ± 1.0 °C) and salinity (1.5; refractometric measurements) were measured directly *in situ*. Samples were conserved at 4 °C during transport to the laboratory.

2.2. Bed elevation and suspended sediments recording

The bed level variation of Tancarville mudflat was monitored by an altimeter deployed in station A. The "Altus" device consists of a non-disturbing submersible acoustic sensor with sub-millimeter resolution fixed above the SWI. It is also equipped with a pressure sensor to measure the height of water above the mudflat (Deloffre et al., 2005). This method has already been used for geochemical studies in dynamic environments to account for short term erosion/deposition processes (*e.g.,* Bally et al., 2004; Denis et al., 2009). In order to observe the erosive dynamics during flood tides, bed elevation was measured every 30 s. Flood erosion depth for each tide is obtained from this elevation chronicle.

The suspended sediment concentration (SSC) variation was initially supposed to be determined using a turbidimeter at station A, but there was a lack of recording. To overcome this defect turbidity data from automated monitoring network (SYNAPSES; seine-aval.fr/synapses/) were used. SYNAPSES station is equipped with YSI 6600 V2 multi-parameter probe, recording every 5 min the turbidity 1 m above the bed at station S (Fig. 1). Conversion to SSC is done according to the calibration coefficient of 1.34 mg l^{-1} NTU^{-1} described by Druine et al. (2018) with a relative error of ±47%.

2.3. Physicochemical characterization

Two sediment cores (8 cm inner diameter, 30 cm long) were extracted for *in situ* observations. One was split lengthwise for a visual description of lithofacies and macrofauna activity. Temperature and

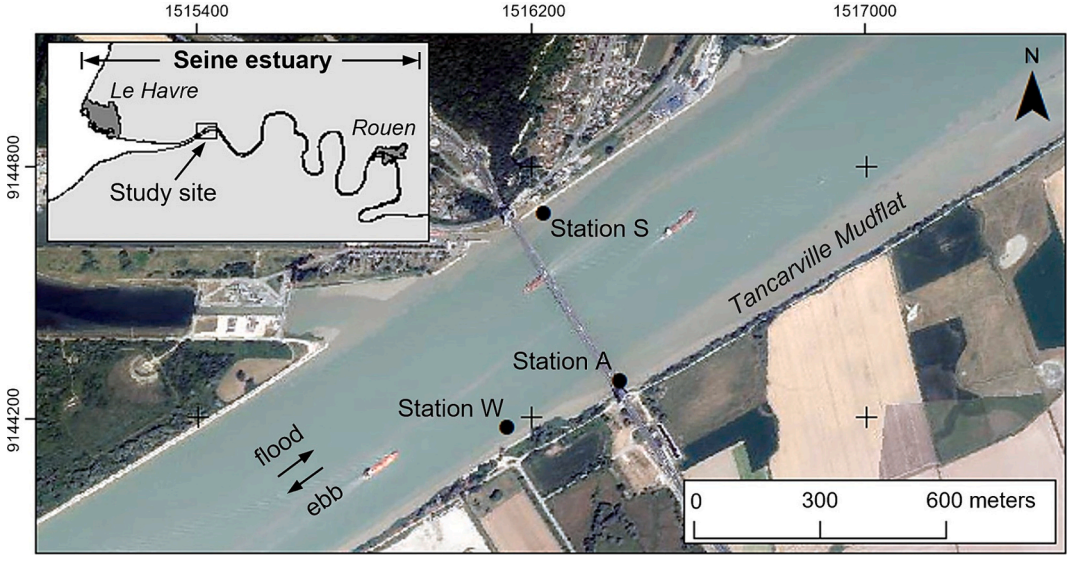

Fig. 1. Location of monitoring and sampling stations near to Tancarville mudflat (coordinate system: RGF Lambert CC50).

redox potential were measured by inserting horizontally a WTW Series 3110 Pt/Pt–Ag/AgCl electrode into holes drilled in the second cores tube every 5 mm. Measured redox potentials were corrected from the reference hydrogen electrode to determine eH.

Fifteen cores (3 cm inner diameter, 5 cm long) were sliced 1 h after sampling at 5 mm intervals using a piston. Subsamples were mixed in three pools (5 cores each) to ensure an appreciable mass of sediment, then dried at 30 °C at least 72 h. For each depth, porosity, and sediment content (SC) were calculated from the mass difference before and after drying, accounting for salinity and further used for particulate phosphorus (PP) partitioning (see 2.6). Three additional cores (3 cm inner diameter, 5 cm long) were calcined in a muffle furnace at 525 °C for 6 h for an overall estimate of organic matter (OM) content.

2.4. Sediment incubation

To compare with model outputs, PO_4^{3-} flux was also measured using a standard laboratory incubation method (Boynton et al., 2018). A large sediment core (26 cm inner diameter, 30 cm long) was sampled at low tide, retrieved back to the laboratory, immersed in 1 l of water from the study site in an opaque box (to prevent photosynthesis) at *in situ* temperature (14.2 ± 1.0 °C) and left for three days for suspended sediment settling. Before incubation water volume was gently completed to 4.5 l and a magnetic stirring bar ensured constant agitation without disturbing the SWI (the PO_4^{3-} concentration at the start of incubation was close to that of the surface waters sampled, *i.e.*, 3.6 ± 0.5 μM). Note that a compaction of 3 cm was measured from sampling and an intense macrofauna activity was observed. Three samples (4 ml each) were taken every 45 min during 9 h and kept frozen until analysis. Flux of PO_4^{3-} was calculated from overlying water concentration change in time ($r^2 = 0.945$) according to the formula of Santschi et al. (1990), corrected for sample volume.

2.5. DET procedure

Sampling of pore water PO_4^{3-} was carried out using DET (Davison et al., 1991). A polyacrylamide gel (18 cm high, 8 cm wide, 0.92 mm thick after expansion in deionized water) is prepared as described by Jézéquel et al. (2007) and placed in the central depression of a plexiglass support plate. The gel was covered with a protective porous polysulfone membrane (Ø 0.22 μm) fixed with waterproof tape. The device was conserved in a moisture plastic bag at 4 °C until use. In order to better explain PO_4^{3-} distribution, a second probe gel was prepared for simultaneous sampling of dissolved iron (Fe_d). Both probe gels were deoxygenated by nitrogen bubbling during 5 h before deployment to prevent analyte interferences (Carignan, 1984). They were inserted back-to-back into an *ex-situ* microcosm similar to that used for incubation and left 5 h for equilibration (duration based on instructions from Cesbron et al., 2014).

Computer-imaging densitometry method provide a 2D high-resolution measurement of analyte concentrations (Jézéquel et al., 2007). Colorimetric development for PO_4^{3-} and Fe_d analysis was performed as described by Cesbron et al. (2014). Briefly, two 0.46 mm thick gels previously equilibrated with dedicated reagent solution (ascorbic acid 30 mM, sulfuric acid 0.558 M, potassium antimony(III) tartrate hydrate 0.40 mM, and ammonium molybdate tetrahydrate 18.5 mM for PO_4^{3-}; ferrozine 12.2 mM and ascorbic acid 170 mM for Fe_d) are laid on the probe gels immediately after their retrieval. The gel assemblies are covered with a transparent film (cellulose acetate) and left 20 min for colour development before transfer to a flatbed scanner (Canon Canoscan LiDE 120). Scans were achieved at 300 dpi and processed under ImageJ software (Abràmoff et al., 2004). Images were decomposed into primary colors RGB intensities, each being converted to a gray scale image. Only the most sensitive canals were used, respectively red for PO_4^{3-} and green for Fe. Calibration coefficient (PO_4^{3-}: $r^2 = 0.996$, standard deviation = 9.12% or ± 0.07 μM per reflectance unit; Fe_d: $r^2 = 0.998$, standard deviation = 4.90% or ± 0.06 μM per reflectance unit) were deduced by exposing six standard solutions (0 to 45 μM for PO_4^{3-}; 0 to 150 μM for Fe_d) to the same analytical procedure as for probe gels. Final resolution is downgraded to 500 μm to consider the relaxation effect (Harper et al., 1997) and SWI was repositioned with a relative uncertainty of 1 mm (Thibault de Chanvalon et al., 2017). Numerical treatment of DET data is realized using codes from Thibault de Chanvalon et al. (2015).

2.6. Sequential fractionation of particulate phosphorus

Particulate phosphorus partitioning was determined by chemical extraction applied on dried sediment subsamples (after physical characterization step). First, exchangeable PO_4^{3-} (exch-P) was obtained by infinite dilution extrapolation (Aminot and Andrieux, 1996). An aliquot of approximately 0.5 g dry sediment was successively shaken four times for 1 h in deionized water. After each extraction, suspension was centrifuged, pellet was collected for subsequent procedure, and supernatant was sampled for further PO_4^{3-} analysis. Then, inorganic PP was determined according to Golterman and Booman (1988). Iron bound PO_4^{3-} (Fe(OOH) ≈ P) and calcium bound PO_4^{3-} ($CaCO_3$ ≈ P) were extracted at buffered pH = 8 for 45 min and 17 h four times repeated using a mixed Ca-NTA (0.02 M)/dithionite and Na-EDTA (0.05 M), respectively. Afterward, acid soluble organic PO_4^{3-} (ASOP), corresponding to the labile organic P, was removed in sulfuric acid (0.5 M) during 30 min (De Groot, 1990). Lastly, residual organic PO_4^{3-} (ROP) was extracted by mineralization into a mixed persulfate potassium (1 g)/sulfuric acid (2 ml) in autoclave. This last step was repeated on aliquots not submitted to previous extraction to obtain directly total P.

2.7. Sorption batch experiment

A sorption batch experiment was also performed to measure the sorption rate and assess the influence of particle surface properties or water quality (*e.g.,* Aminot and Andrieux, 1996; Van Raaphorst and Kloosterhuis, 1994; Zhu and Wang, 2014). Eight sediment suspensions (0, 0.2, 0.5, 0.8, 1.25, 1.8, 2.5 and 4 g l^{-1}) were prepared by adding dry superficial sediment in water sampled *in situ* (pH = 8.12; T = 14.2 °C; NaCl = 1.5 g l^{-1}; PO_4^{3-} = 4.27 μM). Erlenmeyer flasks were darkened with aluminum to prevent PO_4^{3-} assimilation and magnetic stirring bars allowed maintaining particles in suspension. Stirring was not constant for the 0.5 g l^{-1} suspension and the sediment settled, so the results were not retained to avoid bias. Samples for PO_4^{3-} concentration monitoring were collected at 0, 5, 15, 30, 60, 100 and 180 min (corresponding to flood tide duration), immediately filtered (0.2 μm) to stop solid-liquid interaction and acidified with hydrochloric acid (10^{-2} M). To explore potential release from other PP pool, in addition to sorption processes, ferrous ion (Fe(II)), dissolved calcium (Ca(II)) and dissolved organic carbon (DOC) concentrations were also measured on these same samples as markers of Fe(OOH) ≈ P reduction, $CaCO_3$ ≈ P dissolution and ASOP mineralization, respectively.

2.8. Chemical and statistical analyses

PO_4^{3-} and Fe_d concentrations were both measured by colorimetric reaction in continuous flow analyzer Bran+Luebbe AutoAnalyzer 3. Detection limits were about 0.13 μg P l^{-1} and 0.20 μg Fe_d l^{-1}. DOC and Ca(II) were determined using respectively a TOC-l Shimadzu and a Metrohm 732 IC with a detection limit of 0.19 mg C l^{-1} and 0.12 mg Ca l^{-1}. All measurements were performed with an accuracy under 5%, determined by repeated analysis of standard samples.

As the application conditions for parametric tests were not met, comparisons of means and correlations were carried out with Mann-Whitney and Spearman tests respectively.

2.9. Model description

Dissolved PO_4^{3-} resuspension flux (J_R) is expressed as the sum, integrated from flood erosion to high tide deposition, of components identified (Fig. 2): diffusion stimulation by exposure of deeper sediment layer with higher PO_4^{3-} concentration in the porewater (J_D), pore water mixing with overlying water (J_M) and net adsorption/desorption from suspended sediments (J_K).

$$J_R(x) = \int_{t_0}^{t_f} [J_D(x) + J_M(x) + J_K(x,t)]dt \quad (1)$$

Where J_R is the total dissolved PO_4^{3-} resuspension flux across SWI by tide (mmol P m^{-2} $tide^{-1}$). Note that it can be expressed relative to the immersion time per tide (μmol m^{-2} h^{-1}) for comparison with standard methods; x is the erosion depth during flood (m), boundary conditions are recalculated according to it; t_f is the flood time (s), defined as the time to recover the initial bed level; J_D is the diffusion stimulation (μmol P m^{-2} s^{-1}); J_M is the mixing flux (μmol P m^{-2}); J_K is the net adsorption/desorption flux (μmol m^{-2} s^{-1}); and t is the time since resuspension started (s).

The theoretical diffusive flux for a given flood erosion depth was calculated using the Fick's first law of diffusion adapted to sediment. To solve the equation, it is assumed that PO_4^{3-} concentration at the SWI and the depth over which the vertical gradient is calculated remain constant during flood erosion (respectively 5.82 μM and 3.5 mm, based on the results of DET measurements described below).

$$J_D(x) = -\varphi_{xi} \times Ds\left(PO_4^{3-}\right)_{xi} \times \frac{Cx_{-\Delta h} - Cx_0}{\Delta h} \quad (2)$$

Where φ_{xi} is the sediment porosity (dimensionless) at depth x; $Cx_{-\Delta h} - Cx_0$ is the difference between concentration at SWI and concentration 3.5 mm below x (μM); Δh is the depth over which the vertical gradient is calculated (m); and $Ds\left(PO_4^{3-}\right)_{xi}$ is the diffusion coefficient of PO_4^{3-} in the sediment (m^2 s^{-1}) at depth x calculated as follows:

$$Ds\left(PO_4^{3-}\right)_{xi} = \frac{D_w\left(PO_4^{3-}\right)_{xi}}{\theta^2{}_{xi}} \quad (3)$$

Where $D_w\left(PO_4^{3-}\right)_{xi}$ is the diffusion coefficient of PO_4^{3-} in water (m^2 s^{-1}) at depth x corrected from the Stokes–Einstein formula (Li and Gregory, 1974): $D_w\left(PO_4^{3-}\right)_{xi} = 7.34 + 0.16(T_{xi} - 25)$ with T_{xi} as the sediment temperature (°C) at depth x; and $\theta 2_{xi}$ the tortuosity at depth x calculated from porosity φ_{xi} according to Boudreau (1996): $\theta^2{}_{xi} = 1 - 2ln\varphi_{xi}$.

The mixing flux is estimated by integrating the quantity of PO_4^{3-} in pore water in the eroded sediment layer (Sun et al., 2006):

$$J_M(x) = \int_{x_0}^{x} (C_{xi} \times V_{xi} \times \varphi_{xi})dx \quad (4)$$

Where C_{xi} is the PO_4^{3-} concentration (μM) at depth x; and V_{xi} the volume of sediment (m^3 m^{-2}) at depth x.

Some models are used to describe sorption process. Here we focus on fast sorption kinetics using an empirical model applied on sorption batch experiments data. The net adsorption/desorption flux is expressed as below:

$$J_K(x,t) = \int_{x_0}^{x} (SC_{xi} \times V_{xi})dx \times q_e(t) \quad (5)$$

Where SC_{xi} is the sediment content (g cm^{-3}) at depth x; $qe(t)$ is the quantity of PO_4^{3-} desorbed by a mass unit for a given resuspension time (μmol g^{-1} s^{-1}) calculated as follows: $q_e = k/(t \times SSC)$ with t is the time from resuspension; SSC is the suspended sediment concentration (g l^{-1}) and k is the sorption coefficient deduced from sorption batch experiment. Practical procedure for calculating k is shown in 3.3 and Fig. 5: Changes in PO_4^{3-} concentration in sorption batch experiment were described by logarithmic fitting functions (equation: $k\,ln(t)$; $r^2 > 0.74$). Then, k was obtained for all SSC using a linear correlation between the two parameters ($r = 0.99$; p value $= 3.26\ 10^{-5}$).

Particulate phosphorus input balance is calculated to assess the capacity of sediments to sustain J_R:

$$J_P(x_r) = \int_{x_0}^{x_r} (PP_{xi} \times SC_{xi} \times V_{xi})dx_r \quad (6)$$

Where J_P is the net residual phosphorus flux (μmol m^{-2} $tide^{-1}$); x_r is the net residual erosion/sedimentation height (m). To consider compaction at low tide, it is defined for a tide n as the difference between the bed level at the start of tides n and n + 1. PP is the phosphorus associated with the particulate fraction (μmol g^{-1}).

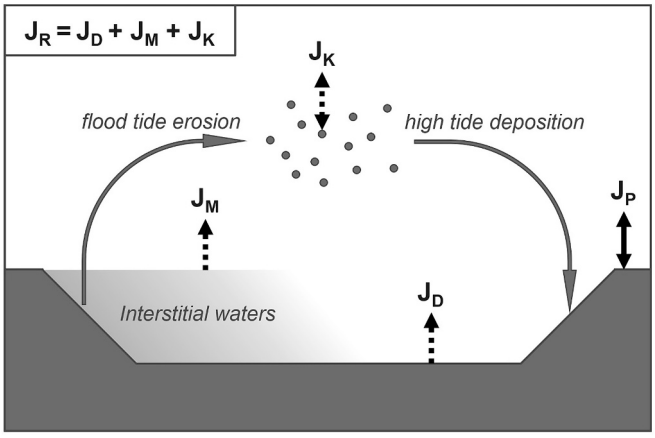

Fig. 2. Conceptual model of dissolved (black dotted arrows) and particulate (black solid arrow) PO_4^{3-} flux components across SWI during tidal resuspension (J_R: dissolved PO_4^{3-} resuspension flux, J_D: diffusion stimulation by exposure of deeper sediment layer with higher PO_4^{3-} concentration in the porewater, J_M: pore water mixing with overlying water, J_K: adsorption/desorption from suspended sediments and J_P: residual erosion/sedimentation).

3. Results

3.1. Mudflat hydro-sedimentary dynamics

Bed level survey of the Tancarville mudflat from 29.03.2022 to 10.05.2022 is shown in Fig. 3a. Except for a short period of net residual erosion the first two days, the mudflat exhibits a 27.7 mm net accretion from 01.04.2022 until the end of the monitoring. Mean erosion depth during flood tide is 2.8 ± 2.5 mm, with some remarkable erosive pulses up to 16.1 mm (Fig. 3a; red bars).

Seine hydro-sedimentary variability above the mudflat is detailed in Fig. 3b. The field survey was carried out while turbidity maximum was back up in the lower estuary, near to study site, in relation to the decrease of Seine water discharge (data not shown). Suspended sediment concentration measured at station S averages 0.44 g l^{-1} during flood tide (Fig. 3b; black points) highlight a strong dependence to the tidal coefficient ($r = 0.98$; p value $<2.2\ 10^{-16}$). Sediment immersion lasts from 6.8 h at spring tide to 9.1 h at neap tide with water height up to 4 m (Fig. 3b; blue line).

3.2. Geochemical and physical features

Fig. 4a shows both dissolved (left panel) and particulate (right panel) analyte concentrations explaining P geochemical behavior in superficial sediments. Concentration of dissolved PO_4^{3-} remains stable at 5.82 ± 2.17 μM until 3 cm depth with a weak gradient of 1.2 ± 6.3 μM cm^{-1} at SWI, then increases progressively until 4.5 cm and sharply up to 22.81 ± 6.90 μM at 5 cm depth (Fig. 4a; red line). Fe_d concentrations follow a

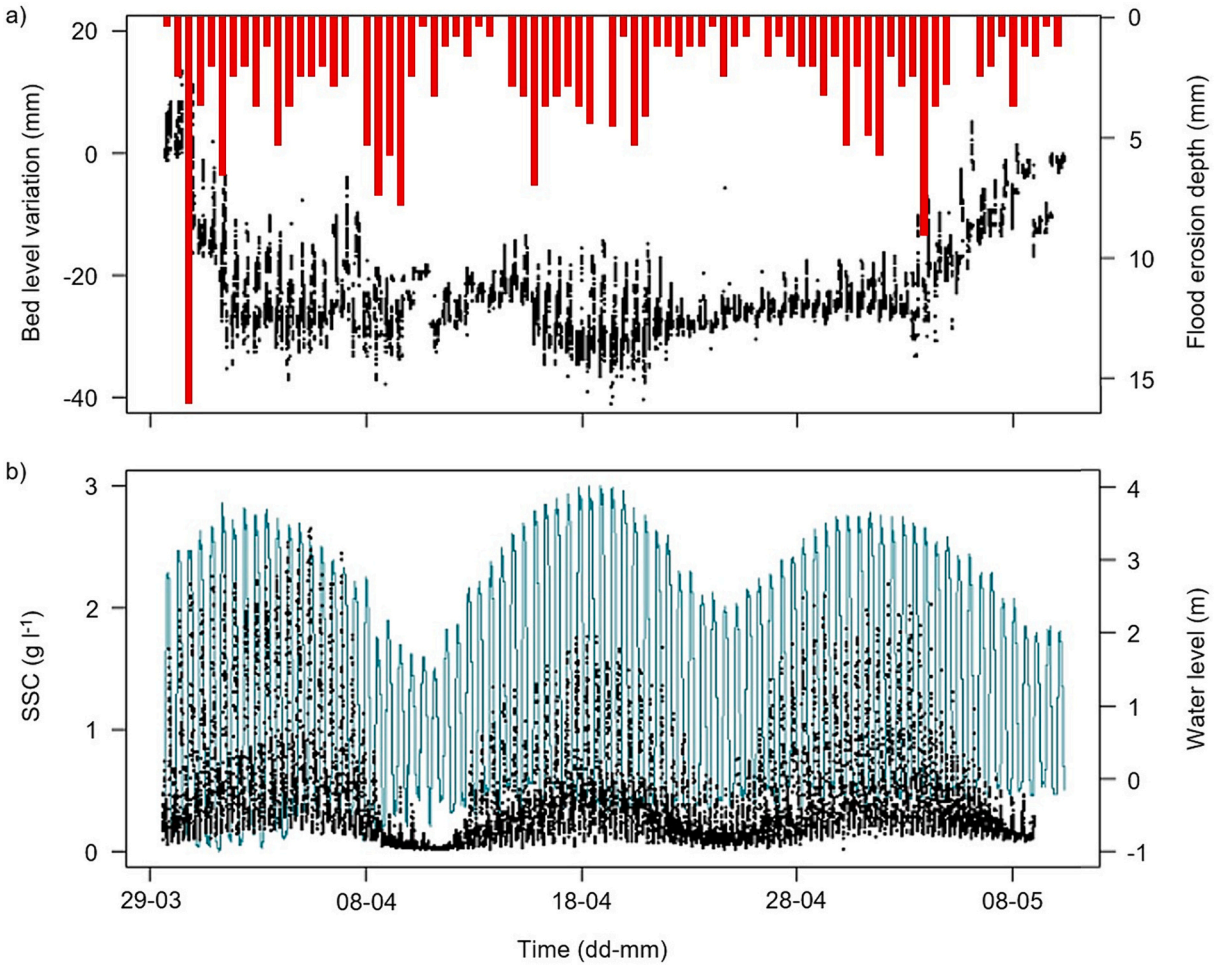

Fig. 3. Monitoring of hydro-sedimentary dynamics on Tancarville mudflat: (a) bed level variation (black points) and the erosion depth during flood tide (red bars). 29-03-2022 bed level is used as the zero reference: (b) Variations of suspended sediment concentration (SSC; black points) and water level (blue line). (For interpretation of the references to colour in this figure legend, the reader is referred to the web version of this article.)

similar distribution to PO_4^{3-} ($r = 0.95$; p value $= 1.86\ 10^{-18}$), with no apparent change down to 3.8 cm depth before increasing sharply until 25.66 ± 15.03 μM at 5 cm depth (Fig. 4a; blue line). Some burrows are visible on the 2D-DET profile in the top 4–5 cm and are associated to low concentration zones. Redox potential decreases continuously from 354 mV to 56 mV (Fig. 4a; black line). Particulate phosphorus content is highly variable, especially in subsurface with an offset exceeding a factor 2 between replicates. Mean Total PP content is 21.85 ± 4.33 μM g^{-1}, of which 1.03 ± 0.21 μM g^{-1} is sorbed (Fig. 4a; black points and blue bars). Inorganic and organic PP account respectively for 62.2 ± 1.7% (28.3 ± 2.0% for Fe(OOH) ≈ P and 34.0 ± 0.7% for $CaCO_3$ ≈ P) and for 32.6 ± 2.1% (18.0 ± 3.2% for ASOP and 14.6 ± 1.4% for ROP).

Sediment physical features are described in Fig. 4b. Temperature and porosity decrease respectively from 13.6 ± 0.3 °C and 0.82 ± 0.06 at subsurface to 12.0 ± 0.4 °C and 0.69 ± 0.10 at 5 cm depth. Inversely, SC increases from 0.84 ± 0.04 g cm^{-3} to 1.08 ± 0.17 g cm^{-3} (Fig. 4b; black points). Polynomial functions are fitted to temperature ($r^2 = 0.99$), porosity ($r^2 = 0.92$), and SC ($r^2 = 0.54$) data for further model implementation (Fig. 4b; black lines). The observation of the core shows that the top 4–5 cm of sediment studied here are millimetric layers of soft sandy-silt deposits, visible despite a high density of oligochaetes. In contrast, sediments deeper than 5 cm are stiff and dark but without sulfur smell (data not shown).

3.3. Empirical modeling of net adsorption/desorption kinetics

The practical procedure applied for q_e modeling from experimental data is illustrated in Fig. 5 (see 2.9 for detailed equation). Results of the sorption batch experiment are shown in Fig. 5a. The Seine water used as solvent has an initial PO_4^{3-} concentration of 4.27 μM and ranges in the blank treatment between 4.09 μM and 4.35 μM (95% confidence interval; Fig. 5a; blue dotted lines). With added sediments, concentrations increase dramatically during the first minutes to one hour, then slowly until they reach 4.52 μM in 0.2 g l^{-1} treatment to 6.23 μM in 4 g l^{-1} treatment after 3 h of suspension (Fig. 5a; gray symbols). Note that whatever the SSC, only net desorption is observed on a flood time scale (below we refer to "net desorption" although adsorption is implicitly taken into account by the method used). In contrast, concentrations of Fe(II), Ca(II) and DOC, not vary significantly over 3 h of suspension in any SSC (p value >0.280; data not shown).

q_e is greater in the first 30 min and at low SSC. For example, for a mean SSC of 0.44 g l^{-1}, q_e decreases rapidly from 1.86 nmol g^{-1} s^{-1} to 0.1 nmol g^{-1} s^{-1} after 30 min of experimentation (Fig. 5c; false colors).

3.4. Model implementation

Fig. 6 illustrates a detailed example of model implementation on a typical tide of 11.04.2022. It is chosen because (1) its flood erosion depth is representative of the whole record and (2) the field sampling, from which some boundary conditions are determined, was conducted

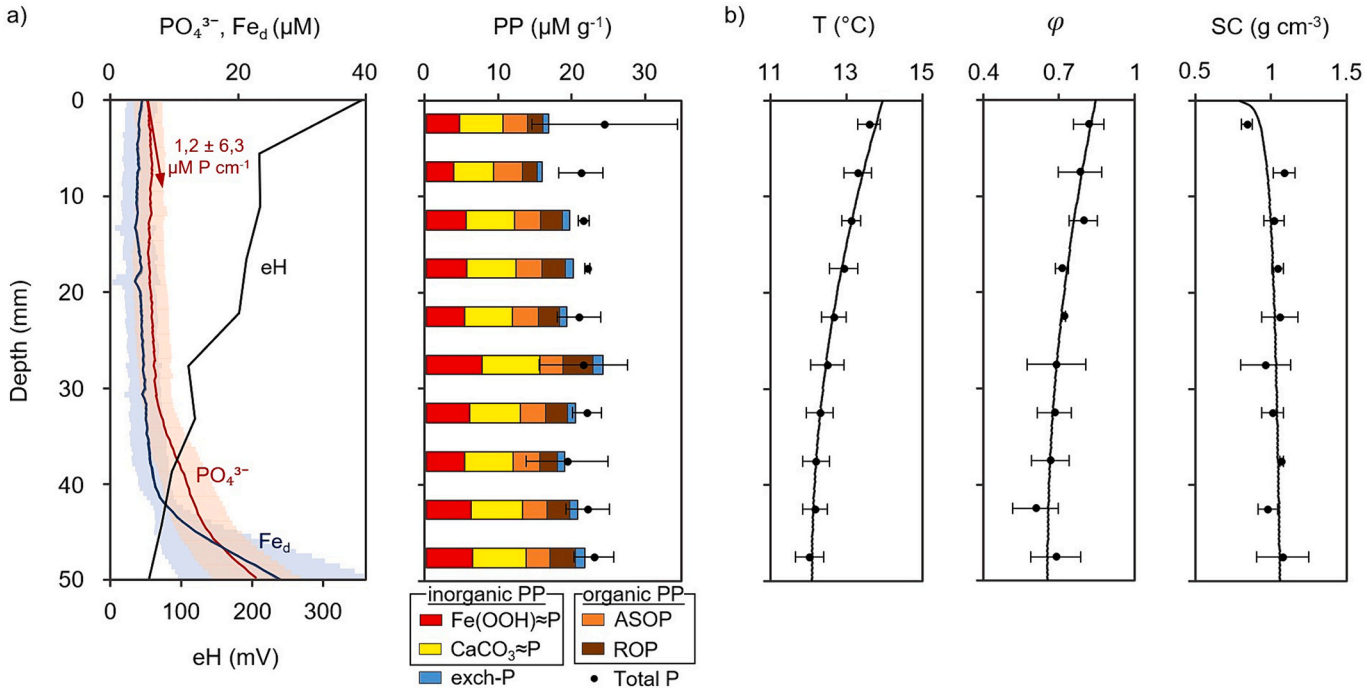

Fig. 4. Profiles of superficial sediment geochemical and physical features: (a) redox potential, PO_4^{3-} and Fe_d concentration (left panel; PO_4^{3-} vertical gradient at SWI is represented by a red arrow and standard deviation by colored area), particulate phosphorus partitioning (related captions; right panel); (b) temperature, porosity, and sediment content. Fitting functions are represented by black lines. (For interpretation of the references to colour in this figure legend, the reader is referred to the web version of this article.)

on the same day. The model is applied on a focus period including the flood tide, with 3.3 mm erosion depth, until the bed level recovers its initial level at high tide (Fig. 6a; shaded area). We assume that resuspension during ebb tide is not taken into account, because it only concerns recent high tide deposits (*e.g.,* interstitial water mixed during the ebb tide is superficial water trapped within the hour and is therefore not attributable to the mudflat). Model output decomposed is zoomed in Fig. 6b. The stimulated diffusive flux J_D is 0.05 nmol m^{-2} s^{-1}, negligible compared with other components, and is not enhanced by erosion (Fig. 6b; green line). The mixing flux J_M flux occurs in pulses up to 4.21 μmol m^{-2} s^{-1}, during which it is temporarily dominant (Fig. 6b; red line). Considering an SSC of 0.21 g l^{-1}, the net desorption flux J_K varies from 0.02 to 2.66 μmol m^{-2} s^{-1} and account for 99.56% of the total flux (Fig. 6b; blue line). The dissolved resuspension flux J_R reaches 3.96 mmol m^{-2} $tide^{-1}$ (Fig. 6b; black line).

The same procedure is applied to the full data record, and the model output is shown in Fig. 7. J_R ranges from 0 mmol m^{-2} $tide^{-1}$ when no erosion is measured, to 13.19 mmol m^{-2} $tide^{-1}$ for the erosive event of 30.03.2022 (Fig. 7; black bars). Relative to the immersion time, J_R is 272.3 ± 360.0 μmol m^{-2} h^{-1}. Flood erosion depth is a good descriptor of J_R, driven by several highly erosive spring tides (Fig. 7; $r = 0.75$; p value $= 1.9\ 10^{-11}$). However, some remarkable J_R are also modeled at neap tide while flood erosion depth is lower (Fig. 7; $r = 0.41$; p value $= 0.001$). It may be related to a longer t_f ($r = 0.86$; p value $= 2.4\ 10^{-14}$) and lower SSC, which favors desorption.

4. Discussion

4.1. Importance of resuspension pathway

To assess the necessity of considering the resuspension pathway, model results are compared with fluxes calculated by standard methods. Reported PO_4^{3-} flux measurements at SWI in Seine are summarized in Table 1. The diffusive PO_4^{3-} flux, determined from classic application of the first Fick's law on the 2D-DET profiles, is 0.15 ± 0.85 μmol m^{-2} h^{-1} (Table 1). It is much lower than previous results (Bally et al., 2004; Table 1) before improvement of the Seine's trophic status (Morelle, 2020), but consistent with recent observations on a mudflat downstream of our study site (Vennin, 2018; Table 1). Meanwhile, the PO_4^{3-} flux deduced by core incubation is 40.8 μmol m^{-2} h^{-1} (Table 1). It is similar to PO_4^{3-} flux reported in various estuarine and coastal systems (Boynton et al., 2018; Table 1), and in Seine upstream (Garban et al., 1995; Table 1). A gap of this magnitude between diffusive flux and incubation results is common (Matisoff et al., 2016) and often associated with high macrofauna density (Forja and Gómez-Parra, 1998) allowing bio-irrigation through their burrow networks (Thibault de Chanvalon et al., 2017). In comparison, and subject to model validation (see below), J_R reaches 1852 μmol m^{-2} h^{-1} (Table 1). It is significantly higher than diffusive flux (p value $<2.2\ 10^{-16}$) and on average 7-fold higher than incubation flux (lack of replicates not permitting statistical testing). A considerable increase in PO_4^{3-} concentrations in water column following resuspension has already been observed in *ex situ* mesocosms (*e.g.,* Sun et al., 2006; Yu et al., 2017) and *in situ* in close water (Zhu et al., 2005), but here we provide the first estimation of the PO_4^{3-} flux following a natural resuspension in open waters from *in situ* data. This model can be applied to longer data chronicles, including extreme events and contrasting hydrological seasons, to provide balances at various scales.

Morelle (2020) estimated the annual input from Seine watershed to the estuary at 1412 ± 539 t PO_4^{3-}. Considering that Seine estuarine mudflats represent approximatively a total of 1000 ha (estimation from seine-aval.fr), PO_4^{3-} recycled *via* resuspension can represent a larger source than external dissolved inputs. Moreover, the modeled PO_4^{3-} advective flux is of the same order as J_R (Vennin, 2018; Table 1). The increase in pressure during flood tide generates a high negative advective flux, which can compensate for that generated by resuspension. It appears necessary in future model implementation in dynamic systems to couple advective and resuspension fluxes.

Changes in turbidity maximum location related to Seine River flow variations control sedimentation in the lower estuary (Deloffre et al., 2006). The field survey was carried out at low water (378 m^{-3} s^{-1} on

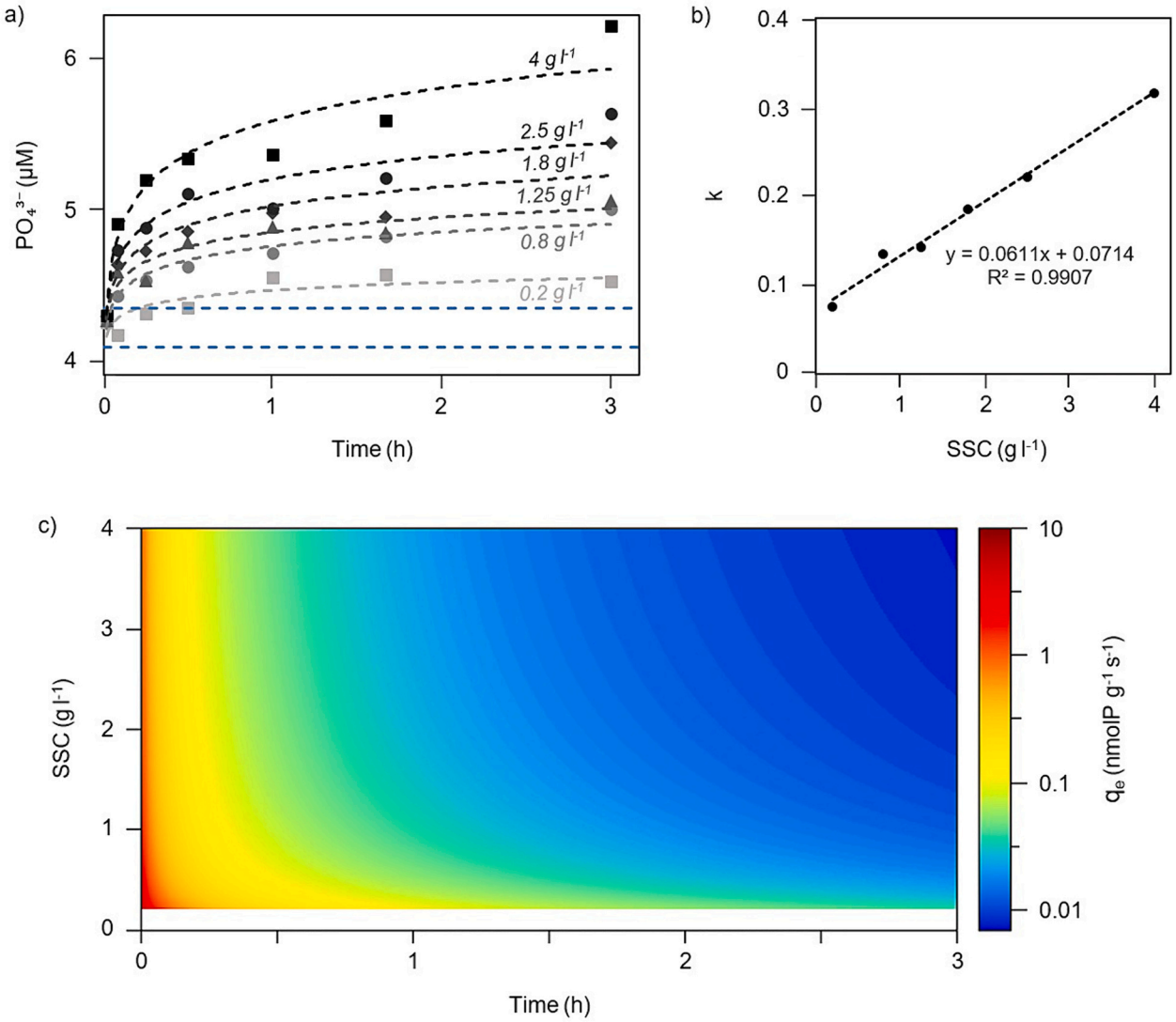

Fig. 5. Net desorption kinetics modeling applied on experimental dataset: (a) evolution of PO_4^{3-} concentrations during sorption batch experiment. A logarithmic function is fitted to the measured data (gray dotted lines). The variability without sediment input is represented by blue dotted lines; (b) linear relationship between k and SSC; (c) q_e for all SSC in false colors. (For interpretation of the references to colour in this figure legend, the reader is referred to the web version of this article.)

average), while maximum turbidity was located close to the study site (data not shown). In consequence, a net accretion of 27.7 mm is observed from 01.04.2022 to the end of the recording (Fig. 3a). Furthermore, the maximum PP content of 38.8 µmol g^{-1} is measured at SWI, suggesting a supply from suspended sediments (Fig. 4a). In order to evaluate the capacity of mudflat to sustain J_R, a PP mass balance is performed (see 2.9). J_P is −823.1 µmol m^{-2} h^{-1} during sedimentation period, high enough to supply modeled J_R. Fresh OM input associated with the migration of turbidity maximum is known to be a seasonal driver of PO_4^{3-} recycling in this part of the Seine estuary (Bally et al., 2004). Under different hydrologic conditions – *i.e.*, when the mudflat is experiencing net erosion – model results can be very divergent.

4.2. Relative importance of transport processes

Suboxic conditions resulting from frequent resuspension in dynamic environments allow efficient degradation of OM (Aller, 1998). However, dissolved PO_4^{3-} content in superficial sediments remained low while OM and ASOP are respectively 4.3 ± 0.2% and 3.48 ± 0.21 µmol g^{-1} (Fig. 4a). It is recognized that mineralization is not sufficient to explain PO_4^{3-} distribution due to its affinity for the solid phase (*e.g.*, Froelich et al., 1979; Bally et al., 2004). For example, $CaCO_3$ ≈ P is the main fraction of PP (Fig. 4a), which can be explained by the high carbonate content of the Seine sediments (30% - 35%; Ouddane et al., 2001). Here, observations suggest that PO_4^{3-} distribution is largely controlled by iron behavior. Reduction of Fe(III) to soluble Fe(II) occurs at a redox potential of about 60 mV (Reeburgh, 1983), similar to redox conditions encountered below 4 cm depth (73 mV; Fig. 4a). Furthermore, Fe(OOH) ≈ P content is 5.62 ± 1.04 µmol g^{-1} (Fig. 4a). Downward transition to anoxic conditions therefore coincided with the simultaneous increase in Fe_d and PO_4^{3-} concentrations (Fig. 4a) and has already been extensively documented (*e.g.*, Cesbron et al., 2014; Thibault de Chanvalon et al., 2015; Gao et al., 2020). Inversely, PO_4^{3-} concentration does not vary significantly in the superficial 3 cm of sediment (p value = 0.299; Fig. 4a) resulting in a very weak vertical gradient of PO_4^{3-} within this depth. Flood resuspension (Caetano et al., 1997) and bioirrigation (Thibault de Chanvalon et al., 2017) can play an important role in oxidant penetration and subsequent formation of an "iron curtain" preventing PO_4^{3-} diffusion (Gao et al., 2020). Thus, there is no apparent stimulation of diffusive flux for pluri-millimeter erosion depths measured on the Tancarville mudflat, J_D accounted in total for <0.001% of J_R (Fig. 6b). For the same reason, J_M accounted for <0.5% of J_R, lower than estimates from Sun et al. (2006). Nevertheless, note that in anoxic conditions with a thinner iron curtain, J_D and J_M can be more important.

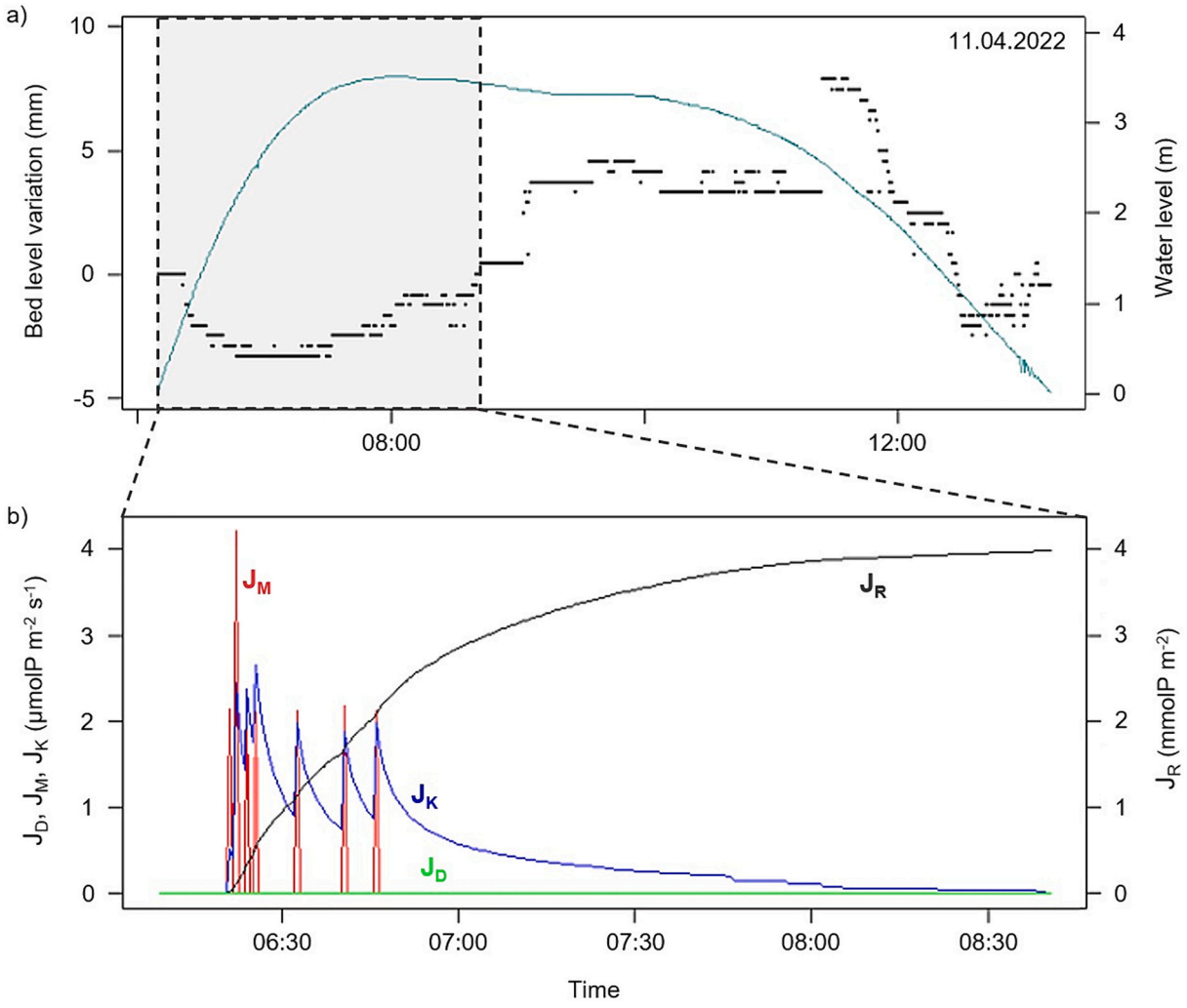

Fig. 6. Graphical example of model application: (a) bed level variation (black points) and water level (blue line) during a typical tide on 11-04-2022. The shaded area represents the focus period; (b) J_D, J_M, J_K (colored lines) and J_R (black line) during flood erosion. (For interpretation of the references to colour in this figure legend, the reader is referred to the web version of this article.)

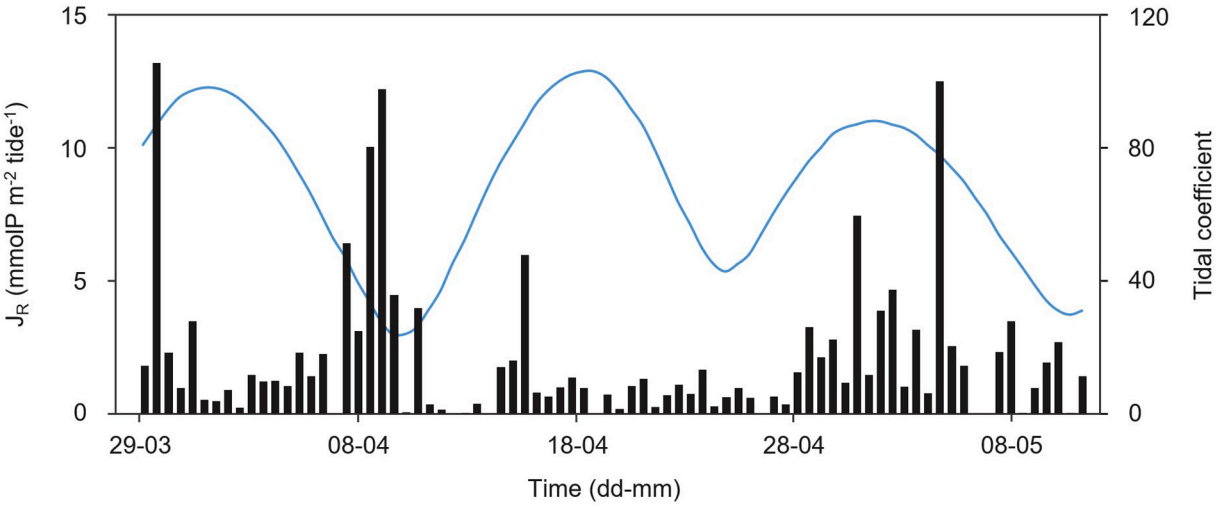

Fig. 7. Model output (black bars) and tidal coefficient (blue line) for each tide during instrumentation of Tancarville mudflat. (For interpretation of the references to colour in this figure legend, the reader is referred to the web version of this article.)

Table 1
Ranges (min to max) of reported PO_4^{3-} flux at SWI for Seine upstream (1), Seine estuary (2) and global review (3). Results are converted in common units.

References	J (μmol m^{-2} h^{-1})	Method
Garban et al., 1995 [1]	44–90	*In situ* incubation
Bally et al., 2004 [2]	13–33	Fick's law (peeper)
Vennin, 2018 [2]	0–1	Fick's law (peeper)
	−1890–1848	Advection model
Boynton et al., 2018 [3]	−230–900	Incubation
	−0.7–1.0	Fick's law (DET)
This study [2]	40.8	*Ex situ* incubation
	0–1852	J_R model

Relatively to other components, J_K is the main pathway of dissolved PO_4^{3-} resuspension flux, supporting the results from Zhu and Wang (2014). The extent of J_R is therefore largely controlled by hydro sedimentary parameters including flood erosion depth, t_f and SSC.

On the flood time scale, 73 ± 23% of exch≈P content is desorbed implying a readjustment between PP pools following resuspension. Likewise, Froelich (1988) observed that fast desorption kinetics accounted for 50 to 90% of the total long-term desorption. To investigate potential release during resuspension from other - less reactive - PP pool, changes in metabolite concentrations are also measured (*e.g.*, Fe (II), Ca(II) and DOC) but these parameters do not vary significantly over 3 h of suspension (p value >0.280). This suggests that Fe(OOH) ≈ P reduction, $CaCO_3$ ≈ P dissolution or ASOP mineralization (if they occur) do not significantly contribute to flux from suspended sediments, at least on the flood time scale.

4.3. Model uncertainty assessment

The most efficient way to assess the robustness of model is to apply it under controlled conditions for validation testing (*i.e.*, Yu et al., 2017). A dynamic mesocosm is actually under development for this purpose. By default, the sensitivity of the model to the parameter uncertainty is computed for a typical tide (flood erosion depth = 2.5 mm; SSC = 0.44 g l^{-1}; t_f = 1 h), and results are summarized in Table 2. In this way, J_R ranges from 1.10 to 2.84 mmol m^{-2} $tide^{-1}$ corresponding to a relative uncertainty of ±52% (Table 2). In contrast, relative uncertainties on J_D and J_M estimates are only ±17% and ± 15%, respectively, and have a negligible effect on the total model uncertainty considering their low relative importance (Table 2). Total uncertainty is mainly driven by two of the J_K boundary conditions (Table 2): (1) Altus resolution (± 0.6 mm; Deloffre et al., 2005), which is relatively important given the low erosion heights involved; and even more (2) the relative error of turbidimeter calibration (± 47%; Druine et al., 2018). In addition, turbidity data from the SYNAPSES network are acquired on the opposite shore to the study site and 1 m above the bed (Fig. 1). However, turbidity decreases sharply with distance from the mudflat (Whitehouse et al., 2000), leading to a certain underestimation of SSC and therefore an overestimation of J_K. It is impossible to precisely quantify this bias, but for a hypothetical underestimation of a factor 10 on SSC measurement, J_K remains the largely dominant component and J_R is still higher than the flux deduced by standard methods (Fig. 8). Thus, particular attention should be paid to turbidity measurement in future implementations.

There are also some unquantifiable biases in model conception and application. For example, to solve the equation of J_D and J_M it is assumed that the PO_4^{3-} profile does not fluctuate during resuspension. Nevertheless, advection (Vennin, 2018) and oxygen dynamics at tidal scale (Denis et al., 2012) can rapidly reshape the PO_4^{3-} profile and affect the model response. To evaluate pore water PO_4^{3-} reactivity during resuspension, the use of a high temporal resolution method (*i.e.*, PO_4^{3-} microelectrode; Lee et al., 2009) or a transient state model (*i.e.*, Denis et al., 2009) is required. However, note that biases on J_D and J_M modeling have low quantitative impact on J_R. Therefore, efforts must be focused on reducing biases related to J_K modeling, considering their relative importance. Sorption processes are controlled by (1) particle surface properties (Zhu and Wang, 2014) and (2) physicochemical characteristics of the solvent (Aminot and Andrieux, 1996). (1) Deflocculation during resuspension can lead to a subsequent re-adsorption (Sun et al., 2006) and reduce net residual PO_4^{3-} flux (You et al., 2007). Here, flocs are gently disaggregated with a pestle to standardize sorption batch experiments, so that flocs behavior is not considered. Turbulence induces aggregation or floc breakup (Winterwerp, 2002)

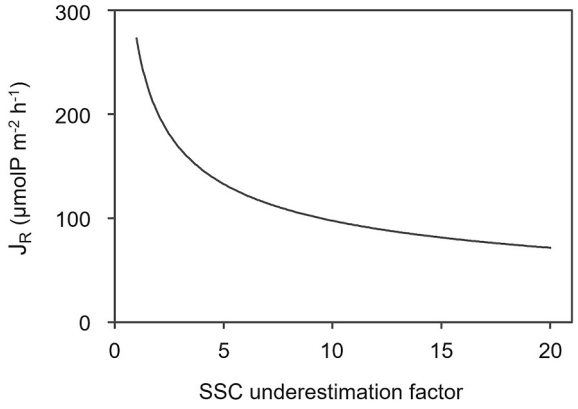

Fig. 8. Dissolved PO_4^{3-} resuspension flux bias in function of SSC underestimation factor.

Table 2
Estimation of model sensitivity from parameter uncertainties for a typical tide (flood erosion depth = 2.5 mm; SSC = 0.44 g l^{-1}; t_f = 1 h). Note the unit difference between components. Total uncertainty is highlighted. Source of parameter uncertainties used is reported.

Range of parameter uncertainty		Model sensitivity			
		J_D (μmol m^{-2} h^{-1})	J_M (μmol m^{-2})	J_K (mmol m^{-2})	J_R (mmol m^{-2})
Temperature [1]	13,3–13,9 °C	0.18–0.19	–	–	–
Porosity [1]	0,77–0,89	0.15–0.22	11.79–13.62	–	–
PO_4^{3-} gradient [2]	150–158 μM m^{-1}	0.18–0.19	–	–	–
PO_4^{3-} concentration [3]	5,56–6,68 μM	–	12.02–13.38	–	–
Sediment content [1]	0,89–0,96 g cm^{-3}	–	–	1.59–1.72	–
SSC [4]	0,23–0,65 g l^{-1}	–	–	1.27–2.75	–
Erosion depth [5]	2,2–2,8 mm	0.18–0.19	10.84–14.57	1.27–2.04	–
Quadratic sum		0.16–0.22	11.55–14.17	1.11–2.82	**1.10–2.84**
Relative Uncertainty		± 17%	± 15%	± 52%	**± 52%**

[1] Standard deviation (from Fig. 4).
[2] Uncertainty on interface placement (± 1 mm; Thibault de Chanvalon et al., 2017).
[3] Standard deviation of DET calibration slope (± 4.9%; see 2.5).
[4] Mean relative error of turbidimeter calibration (± 47%; Druine et al., 2018).
[5] Altus resolution (± 0.6 mm; Deloffre et al., 2005).

and can therefore, for example, serve as a flocculation proxy to further model improvements (an acoustic doppler velocimeter can be easily deployed *in situ* for continuous recording; Verney et al., 2007). (2) Variations in pH, salinity, temperature, and dissolved oxygen concentration influence sorption processes (Aminot and Andrieux, 1996) and floc behavior (Mietta et al., 2009). Here, the water used as solvent for the sorption batch experiment is sampled 300 m downstream of the study site during resuspension, to provide the more realistic conditions. But sampling is carried out at neap tide, while water quality fluctuates as a function of tide coefficient (data not shown; seine-aval.fr/synapses/). Additional measurements are required to select the significant parameters, because it is technically complicated to acquire simultaneously so many boundary conditions.

5. Conclusion

A model for *in situ* measurements of dissolved PO_4^{3-} resuspension flux is described and applied over 80 tidal cycles from a Seine estuarine mudflat. Model outputs allowed to describe (1) qualitatively and (2) quantitatively the processes involved. (1) Suboxic conditions in superficial sediments (> 60 mV) resulting from frequent resuspension and intensive bioirrigation buffer dissolved PO_4^{3-} concentrations by enhancing co-precipitation with iron hydroxides. Thus, for a flood erosion ranging from 0 to 16.1 mm, the contribution of diffusion across SWI and pore water mixing are negligible (< 0.0001% and 0.5% respectively). Conversely, net desorption from suspended sediments appears to be the main component despite substantial overestimation due to turbidity measurement procedure. (2) Total dissolved PO_4^{3-} resuspension flux is 272.3 ± 360.0 μmol m^{-2} h^{-1} (± 52% from parameter uncertainty), several times higher than PO_4^{3-} flux deduced by application of first Fick's law of diffusion on DET profiles (0.15 ± 0.85 μmol m^{-2} h^{-1}) or by *ex situ* core incubation (40.8 μmol m^{-2} h^{-1}). To control and improve the robustness of the model, an application under controlled conditions can be performed. Moreover, for an exhaustive estimation of the PO_4^{3-} flux at SWI in a dynamic environment, the approach presented here can be coupled with an advection model. Overall, our results imply that resuspension is one of the main pathways of PO_4^{3-} flux at SWI in dynamic environments and can exceed river inputs. A better understanding of the role of sediments in nutrient cycling is needed to model the evolution of biogeochemical processes in a context of reduced external inputs.

CRediT authorship contribution statement

Jean-Marie Barrois: Conceptualization, Data curation, Formal analysis, Investigation, Methodology, Visualization, Writing – original draft, Writing – review & editing. **Valérie Mesnage:** Funding acquisition, Project administration, Resources, Supervision, Writing – review & editing. **Edouard Metzger:** Methodology, Supervision, Writing – review & editing. **Dominique Mouazé:** Supervision, Writing – review & editing. **Lionel Denis:** Writing – review & editing. **Julien Deloffre:** Methodology.

Data availability

Data will be made available on request.

Acknowledgments

This research was partially supported by the "INTERFACE 2M" EC2CO CNRS Program. The authors would like to thanks David Moussa who performed part of the chemical analysis and reviewer for their valuable recommendations to improve this manuscript.

References

Abràmoff, M.D., Magalhães, P.J., Ram, S.J., 2004. Image processing with ImageJ. Biophoton. Int. 11 (7), 36–42.
Aller, R.C., 1998. Mobile deltaic and continental shelf muds as suboxic, fluidized bed reactors. Mar. Chem. 61 (3–4), 143–155.
Aminot, A., Andrieux, F., 1996. Concept and determination of exchangeable phosphate in aquatic sediments. Water Res. 30 (11), 2805–2811.
Bally, G., Mesnage, V., Deloffre, J., Clarisse, O., Lafite, R., Dupont, J.P., 2004. Chemical characterization of porewaters in an intertidal mudflat of the seine estuary: relationship to erosion–deposition cycles. Mar. Pollut. Bull. 49 (3), 163–173.
Boudreau, B.P., 1996. The diffusive tortuosity of fine-grained unlithified sediments. Geochim. Cosmochim. Acta 60 (16), 3139–3142.
Boynton, W.R., Hagy, J.D., Cornwell, J.C., Kemp, W.M., Greene, S.M., Owens, M.S., Baker, J.E., Larsen, R.K., 2008. Nutrient budgets and management actions in the Patuxent River estuary, Maryland. Estuar. Coasts 31, 623–651.
Boynton, W.R., Ceballos, M.A.C., Bailey, E.M., Hodgkins, C.L.S., Humphrey, J.L., Testa, J. M., 2018. Oxygen and nutrient exchanges at the sediment-water interface: a global synthesis and critique of estuarine and coastal data. Estuar. Coasts 41 (2), 301–333.
Caetano, M., Falcao, M., Vale, C., Bebianno, M.J., 1997. Tidal flushing of ammonium, iron and manganese from inter-tidal sediment pore waters. Mar. Chem. 58 (1–2), 203–211.
Carignan, R., 1984. Interstitial water sampling by dialysis: methodological notes. Limnol. Oceanogr. 29 (3), 667–670.
Cesbron, F., Metzger, E., Launeau, P., Deflandre, B., Delgard, M.L., Thibault de Chanvalon, A., Geslin, E., Anschutz, P., Jézéquel, D., 2014. Simultaneous 2D imaging of dissolved iron and reactive phosphorus in sediment porewaters by thin-film and hyperspectral methods. Environ. Sci. Technol. 48 (5), 2816–2826.
Davison, W., Grime, G.W., Morgan, J.A.W., Clarke, K., 1991. Distribution of dissolved iron in sediment pore waters at submillimetre resolution. Nature 352 (6333), 323–325.
De Groot, C.J., 1990. Some remarks on the presence of organic phosphates in sediments. Hydrobiologia 207 (1), 303–309.
Deloffre, J., Lafite, R., Lesueur, P., Lesourd, S., Verney, R., Guézennec, L., 2005. Sedimentary processes on an intertidal mudflat in the upper macrotidal seine estuary, France. Estuar. Coast. Shelf Sci. 64 (4), 710–720.
Deloffre, J., Lafite, R., Lesueur, P., Verney, R., Lesourd, S., Cuvilliez, A., Taylor, J., 2006. Controlling factors of rhythmic sedimentation processes on an intertidal estuarine mudflat—role of the turbidity maximum in the macrotidal seine estuary, France. Mar. Geol. 235 (1–4), 151–164.
Denis, L., Boust, D., Thouvenin, B., Le Hir, P., Deloffre, J., Gonzalez, J.L., Gillet, P., 2009. 15 Dynamic Diagenetic Modelling and Impacts of Biota. Environmental Assessment of Estuarine Ecosystems: A Case Study, p. 303.
Denis, L., Gevaert, F., Spilmont, N., 2012. Microphytobenthic production estimated by in situ oxygen microprofiling: short-term dynamics and carbon budget implications. J. Soils Sediments 12 (10), 1517–1529.
Druine, F., Verney, R., Deloffre, J., Lemoine, J.P., Chapalain, M., Landemaine, V., Lafite, R., 2018. In situ high frequency long term measurements of suspended sediment concentration in turbid estuarine system (seine estuary, France): optical turbidity sensors response to suspended sediment characteristics. Mar. Geol. 400, 24–37.
Dunn, R.J., Waltham, N.J., Teasdale, P.R., Robertson, D., Welsh, D.T., 2017. Short-term nitrogen and phosphorus release during the disturbance of surface sediments: a case study in an urbanised estuarine system (gold coast broadwater, Australia). J. Marine Sci. Eng. 5 (2), 16.
Forja, J.M., Gómez-Parra, A., 1998. Measuring nutrient fluxes across the sediment-water interface using benthic chambers. Mar. Ecol. Prog. Ser. 164, 95–105.
Froelich, P.N., 1988. Kinetic control of dissolved phosphate in natural rivers and estuaries: a primer on the phosphate buffer mechanism 1. Limnol. Oceanogr. 33 (4part2), 649–668.
Froelich, P., Klinkhammer, G.P., Bender, M.L., Luedtke, N.A., Heath, G.R., Cullen, D., Dauphin, P., Hammond, D., Hartman, Maynard, V., 1979. Early oxidation of organic matter in pelagic sediments of the eastern equatorial Atlantic: suboxic diagenesis. Geochim. Cosmochim. Acta 43 (7), 1075–1090.
Gao, L., Li, R., Liang, Z., Yan, C., Zhu, A., Li, S., Yang, Z., He, H., Gan, H., Chen, J., 2020. Remobilization mechanism and release characteristics of phosphorus in saline sediments from the Pearl River estuary (PRE), South China, based on high-resolution measurements. Sci. Total Environ. 703, 134411.
Garban, B., Ollivon, D., Poulin, M., Gaultier, V., Chesterikoff, A., 1995. Exchanges at the sediment-water interface in the river seine, downstream from Paris. Water Res. 29 (2), 473–481.
Golterman, H.L., Booman, A., 1988. Sequential extraction of iron-phosphate and calcium-phosphate from sediments by chelating agents: with 4 tables in the text. Int. Vereinigung für theoretische und angewandte Limnologie: Verhandlungen 23 (2), 904–909.
Harper, M.P., Davison, W., Tych, W., 1997. Temporal, spatial, and resolution constraints for in situ sampling devices using diffusional equilibration: dialysis and DET. Environ. Sci. Technol. 31 (11), 3110–3119.
Huettel, M., Berg, P., Kostka, J.E., 2014. Benthic exchange and biogeochemical cycling in permeable sediments. Annu. Rev. Mar. Sci. 6, 23–51.
Hulot, V., Metzger, E., Thibault de Chanvalon, A., Mouret, A., Schmidt, S., Deflandre, B., Rigaud, S., Beneteau, E., Savoye, N., Souchu, P., Le Merrer, Y., Maillet, G.M., 2023. Impact of an exceptional winter flood on benthic oxygen and nutrient fluxes in a temperate macrotidal estuary: potential consequences on summer deoxygenation. Front. Mar. Sci. 10, 1083377.

Jézéquel, D., Brayner, R., Metzger, E., Viollier, E., Prévot, F., Fiévet, F., 2007. Two-dimensional determination of dissolved iron and sulfur species in marine sediment pore-waters by thin-film based imaging. Thau lagoon (France). Estuar. Coast. Shelf Sci. 72 (3), 420–431.
Komada, T., Reimers, C.E., 2001. Resuspension-induced partitioning of organic carbon between solid and solution phases from a river–ocean transition. Mar. Chem. 76 (3), 155–174.
Lafite, R., Romana, L.A., 2001. A man-altered macrotidal estuary: ~ the seine estuary (France): introduction to the special issue. Estuaries 24, 939.
Laima, M.H.C., Matthiesen, H., Lund-Hansen, L.C., Christiansen, C., 1998. Resuspension studies in cylindrical microcosms: effects of stirring velocity on the dynamics of redox sensitive elements in a coastal sediment. Biogeochemistry 43 (3), 293–309.
Lee, W.H., Seo, Y., Bishop, P.L., 2009. Characteristics of a cobalt-based phosphate microelectrode for in situ monitoring of phosphate and its biological application. Sensors Actuators B Chem. 137 (1), 121–128.
Li, Y.H., Gregory, S., 1974. Diffusion of ions in sea water and in deep-sea sediments. Geochim. Cosmochim. Acta 38 (5), 703–714.
Matisoff, G., Kaltenberg, E.M., Steely, R.L., Hummel, S.K., Seo, J., Gibbons, K.J., Bridgeman, T.B., Seo, Y., Behbahani, M., James, W.F., Johnson, L.T., Doan, P., Dittrich, M., Evans, M.A., Chaffin, J.D., 2016. Internal loading of phosphorus in western Lake Erie. J. Great Lakes Res. 42 (4), 775–788.
Mesnage, V., Ogier, S., Bally, G., Disnar, J.R., Lottier, N., Dedieu, K., Rabouille, C., Copard, Y., 2007. Nutrient dynamics at the sediment–water interface in a Mediterranean lagoon (Thau, France): influence of biodeposition by shellfish farming activities. Mar. Environ. Res. 63 (3), 257–277.
Mietta, F., Chassagne, C., Manning, A.J., Winterwerp, J.C., 2009. Influence of shear rate, organic matter content, pH and salinity on mud flocculation. Ocean Dyn. 59, 751–763.
Morelle, J., 2020. Projet SPORES : Synthèse sur les Nutriments et la Production Primaire dans l'estuaire de la Seine. Rapport d'étude réalisé par le GIP Seine-Aval, p. 84.
Ouddane, B., Boust, D., Martin, E., Fischer, J.C., Wartel, M., 2001. The post-depositional reactivity of iron and managanese in the sediments of a macrotidal estuarine system. Estuaries 24 (6), 1015–1028.
Porter, E.T., Owens, M.S., Cornwell, J.C., 2006. Effect of sediment manipulation on the biogeochemistry of experimental sediment systems. J. Coast. Res. 22 (6 (226)), 1539–1551.
Porter, E.T., Manson, R.P., Sanford, L.P., 2010. Effect of tidal resuspension on benthic–pelagic coupling in an experimental ecosystem study. Mar. Ecol. Prog. Ser. 413, 33–53.
Reddy, K.R., Fisher, M.M., Ivanoff, D., 1996. Resuspension and diffusive flux of nitrogen and phosphorus in a hypereutrophic lake. In: American Society of Agronomy, Crop Science Society of America, and Soil Science Society of America, 25, no. 2, pp. 363–371.
Reeburgh, W.S., 1983. Rates of biogeochemical processes in anoxic sediments. Annu. Rev. Earth Planet. Sci. 11 (1), 269–298.
Santschi, P., Höhener, P., Benoit, G., Buchholtz-ten Brink, M., 1990. Chemical processes at the sediment-water interface. Mar. Chem. 30, 269–315.
Schroeder, H., Duester, L., Fabricius, A.L., Ecker, D., Breitung, V., Ternes, T.A., 2020. Sediment water (interface) mobility of metal (loid) s and nutrients under undisturbed conditions and during resuspension. J. Hazard. Mater. 394, 122543.
Sun, X., Zhu, G., Luo, L., Qin, B., 2006. Experimental study on phosphorus release from sediments of shallow lake in wave flume. Sci. China Series D 49 (1), 92–101.
Tengberg, A., Almroth, E., Hall, P., 2003. Resuspension and its effects on organic carbon recycling and nutrient exchange in coastal sediments: in situ measurements using new experimental technology. J. Exp. Mar. Biol. Ecol. 285, 119–142.
Thibault de Chanvalon, A., Metzger, E., Mouret, A., Cesbron, F., Knoery, J., Rozuel, E., Launeau, P., Nardelli, M.P., Jorissen, F.J., Geslin, E., 2015. Two-dimensional distribution of living benthic foraminifera in anoxic sediment layers of an estuarine mudflat (Loire estuary, France). Biogeosciences 12 (20), 6219–6234.
Thibault de Chanvalon, A.T., Metzger, E., Mouret, A., Knoery, J., Geslin, E., Meysman, F. J.R., 2017. Two dimensional mapping of iron release in marine sediments at submillimetre scale. Mar. Chem. 191, 34–49.
Van Raaphorst, W., Kloosterhuis, H.T., 1994. Phosphate sorption in superficial intertidal sediments. Mar. Chem. 48 (1), 1–16.
Vennin, A., 2018. Etude de l'interface eau-sédiment dans les géosystèmes estuariens: approche couplée biogéochimie et modélisation par l'évaluation des flux de nutriments (C, N, P). PhD thesis. Université de Rouen Normandie.
Verney, R., Deloffre, J., Brun-Cottan, J.C., Lafite, R., 2007. The effect of wave-induced turbulence on intertidal mudflats: impact of boat traffic and wind. Cont. Shelf Res. 27 (5), 594–612.
Whitehouse, R.J.S., Soulsby, R.L., Roberts, W., Mitchener, H.J., 2000. Dynamics of Estuarine Muds.
Winterwerp, J.C., 2002. On the flocculation and settling velocity of estuarine mud. Cont. Shelf Res. 22 (9), 1339–1360.
Yang, J., Ma, Y., Li, S., Wang, J., Jin, Z., Li, D., Wang, Y., 2023. Phosphorus release flux and mechanism at the sediment–water interface of the three gorges reservoir in the Yangtze River basin, China. J. Soils Sediments 1–12.
You, B.S., Zhong, J.C., Fan, C.X., Wang, T.C., Zhang, L., Ding, S.M., 2007. Effects of hydrodynamics processes on phosphorus fluxes from sediment in large, shallow Taihu Lake. J. Environ. Sci. 19 (9), 1055–1060.
Yu, Z., Zhong, X., Yu, C., Wang, C., Duan, P., Wen, L., You, Y., 2017. Characteristics of nutrient release from sediments under different flow conditions. Chem. Speciat. Bioavailab. 29 (1), 70–77.
Zhu, H.W., Wang, D.Z., 2014. Relative roles of resuspended particles and pore water in release of contaminants from sediment. Water Sci. Eng. 7 (3), 344–350.
Zhu, G., Qin, B., Gao, G., 2005. Direct evidence of phosphorus outbreak release from sediment to overlying water in a large shallow lake caused by strong wind wave disturbance. Chin. Sci. Bull. 50 (6), 577–582.